Structural and Lithium Ion Transport Studies in Sol−Gel-Prepared Lithium Silicophosphate Glasses†

K. J. Rao,* N. Baskaran, P. A. Ramakrishnan, B. G. Ravi, and A. Karthikeyan

Solid State and Structural Chemistry Unit, Indian Institute of Science, Bangalore-560 012, India

Received March 31, 1998. Revised Manuscript Received July 6, 1998

Lithium silicophosphate glasses have been prepared by a sol−gel route over a wide range of compositions. Their structural and electrical properties have been investigated. Infrared spectroscopic studies show the presence of hydroxyl groups attached to Si and P. MAS NMR investigations provide evidence for the presence of different phosphatic units in the structure. The variations of dc conductivities at 423 K and activation energies have been studied as a function of composition, and both exhibit an increasing trend with the ratio of nonbridging oxygen to bridging oxygen in the structure. Ac conductivity behavior shows that the power law exponent, *s*, is temperature dependent and exhibits a minimum. Relaxation behavior has been examined in detail using an electrical modulus formalism, and modulus data were fitted to Kohlraush−William−Watts stretched exponential function. A structural model has been proposed and the unusual properties exhibited by this unique system of glasses have been rationalized using this model. Ion transport in these glasses appears to be confined to unidimensional conduits defined by modified phosphate chains and interspersed with unmodified silica units.

Introduction

Lithium ion conductors have become very important in view of the developments in lithium battery research.[1−5] At the low end of power requirements of lithium batteries, ease of fabrication is also an important consideration. Glassy electrolytes which exhibit Li ion conductivities of $\approx 10^{-3}-10^{-5}$ S/cm at room temperature have been studied fairly extensively in the literature.[6−17] However, there has been a continuous search for Li electrolyte systems that are glassy and therefore offer inherent advantages such as isotropic conductivity and easiness of fabrication. The sol−gel method of preparation of amorphous materials has been well-documented.[18] Sol−gel routes are also very attractive for preparation of electrolyte films, although very little is reported in the literature regarding the preparation of ion conducting films by this technique.

Ionic conductivities in glasses are quite dependent on the nature and composition of the anion matrix. Also, the introduction of two different types of anions often leads to enhanced conductivities.[19−21] The stabilities and the openness of the structure of the glasses are helped by the presence of polymeric anion formers such as silicates and phosphates. But a well-known observation regarding such polymeric glass formers is that in a combination they cannot be made into glasses easily by the conventional melt-quenching route. Therefore, it is essential that they are prepared by a low-temperature soft chemical route like the sol−gel method. The method also enables introduction of the carrier cations in the form of soluble and easily decomposable salts in aqueous solutions. This strategy has been exploited for the preparation of Li ion conducting glasses.[22−25] The

† This article is dedicated to the memory of Prof. Jean Rouxel whose friendship will be long-remembered.

* Corresponding author: FAX: +91-80-334 1683. Tel: +91-80-344 3897/309 2583. E-mail: kjrao@sscu.iisc.ernet.in.

(1) Tuller, H. L.; Button, D. P.; Uhlmann, D. R. *J. Non-Cryst. Solids* **1980**, *40*, 93.
(2) Angell, C. A. *Solid State Ionics* **1983**, *9−10*, 6.
(3) Kulkarni, A. R.; Maiti, H. S.; Paul, A. *Bull. Mater. Sci.* **1984**, *6*, 201.
(4) Angell, C. A. *Chem. Rev.* **1990**, *90*, 523.
(5) Jones, S. D.; Akridge, J. R. Handbook of Solid-State Batteries and Capacitors; Munshi, M. Z. A., Ed.; World Scientific: Singapore, 1995.
(6) Malugani, J. P.; Robert, G. *Solid State Ionics* **1980**, *1*, 519.
(7) Ribes, M.; Barrau, B.; Souquet, J. *J. Non-Cryst. Solids* **1980**, *38−39*, 271.
(8) Wada, H.; Menetrier, M.; Levasseur, A.; Hagenmuller, P. *Mater. Res. Bull.* **1983**, *18*, 189.
(9) Carette, B.; Robinel, E.; Ribes, M. *Glass Technol.* **1983**, *24*, 147.
(10) Pradel, A.; Ribes, M. *Solid-state Ionics* **1986**, *18−19*, 351.
(11) Kikkawa, S.; Miyai, T.; Koizumi, M. *Solid State Ionics* **1988**, *28−30*, 743.
(12) Konda, S.; Takada, K.; Yamamura, Y. *Solid State Ionics* **1989**, *53−56*, 29.
(13) Kennedy, J. H. *Mater. Chem. Phys.* **1989**, *23*, 29.
(14) Zhang, Z.; Kennedy, J. H. *Solid State Ionics* **1990**, *38*, 217.
(15) Tatsumisago, M.; Hirai, K.; Minami, T.; Tanaka, T.; Kondo, S. *J. Ceram. Soc. Jpn.* **1993**, *101*, 1315.
(16) Rao, K. J.; Ganguli, M. Handbook of Solid-State Batteries and Capacitors; Munshi, M. Z. A., Ed.; World Scientific: Singapore, 1995.
(17) Tatsumisago, M.; Hirai, K.; Minami, T.; Takahashi, M. *Phys. Chem. Glasses* **1997**, *38*, 63.
(18) Hench, L. L.; West, J. K. *Chem. Rev.* **1990**, *90*, 33.
(19) Kunze, D. In *Fast Ion Transport in Solids*; Van Gool, W., Ed.; North-Holland Publishing Company, 1973.
(20) Carette, B.; Ribes, M.; Souquet, J. L. *Solid State Ionics* **1983**, *9−10*, 735.
(21) Chiodelli, G.; Magistris, A. *Solid State Ionics* **1986**, *18/19*, 356.
(22) Hayri, E. A.; Greenblatt, M. *J. Non-Cryst. Solids* **1987**, *94*, 387.
(23) Klein, L. C. *Solid State Ionics* **1989**, *32/33*, 639.
(24) Hayri, E. A.; Greenblat, M.; Tsai, M. T.; Tsai, P. P. *Solid State Ionics* **1990**, *37*, 233.
(25) Munro, B.; Wang, M.; Greenblat, M. *J. Non-Cryst. Solids* **1996**, *196*, 291.

10.1021/cm980216o CCC: $15.00
Published on Web 10/02/1998

topological features of the resulting mixed glass former matrixes and the nature of ion transport in such sol−gel-prepared systems would be very interesting to examine.

Keeping the above consideration in view, we have investigated lithium silicophosphate glasses prepared by the sol−gel route. Our studies include thermal and electrical properties and investigations of structure by infrared (IR) and high resolution magic angle spinning nuclear magnetic resonance (HR MAS NMR) spectroscopic techniques. Ion transport and dielectric studies at various temperatures and frequencies, which often provide valuable suggestive information about the conduction mechanism of the glasses, have been studied in detail in view of the importance of these materials as potential electrolytes for battery applications. A structural model has been proposed which consistently explains the observed behavior.

Experimental Section

Glass Preparation. Lithium silicophosphate glasses were prepared by the sol−gel method. Three series of glasses corresponding to constant phosphorus pentoxide composition (CP), constant lithia composition (CL), and constant silica composition (CS) were prepared with the following prescription.

(i) CP compositions

$$x\ Li_2O/(80 - x)\ SiO_2/20\ P_2O_5 \quad x = 10-40 \text{ in steps of } 10$$

(ii) CL compositions

$$20\ Li_2O/(80 - x)\ SiO_2/x\ P_2O_5 \quad x = 10-30 \text{ in steps of } 5$$

(iii) CS compositions

$$(30 - x)\ Li_2O/70\ SiO_2/x\ P_2O_5 \quad x = 5-20 \text{ in steps of } 5$$

Reagent grade orthophosphoric acid (OPA) (E. Merck), tetraethyl orthosilicate (TEOS) (E. Merck), and lithium nitrate ($LiNO_3$) (E. Merck,) were used as starting materials. Sols were prepared by mixing the three solutions (i) TEOS in ethyl alcohol, (ii) OPA in ethyl alcohol, and (iii) lithium nitrate in water. The solutions were mixed thoroughly using a magnetic stirrer for 3 h to get a uniform sol. Gelation took place after 3−4 days. The gel was then dried at 373 K for 1 week. The dried xerogels were further heat treated at different temperatures and their X-ray diffraction patterns were examined on an X-ray diffractometer. Only the amorphous samples were subjected to further investigations. Densities of the samples were determined using a densitometer and xylene as the displacement fluid. The glasses so prepared were stored in a vacuum desiccator over anhydrous $CaCl_2$.

Thermal Studies. The thermal behavior of gel powders was examined using a Perkin-Elmer differential thermal analyzer (DTA) model 1700. Approximately 20 mg of the sample was sufficient for the investigation in view of the high gains possible on the instrument. Thermograms were recorded from room-temperature up to 1273 K at a typical heating rate of 20 K/min. The operations were computer-controlled and the data were analyzed by Perkin-Elmer software version 3.1. The thermal data was used (see later) to program the necessary heat treatment required for other measurements. We refer to the amorphous gel powders hereafter as glasses, although no clear glass transition was exhibited by these silica-rich silicophosphates, even up to 1273 K.

Spectroscopic Studies. Fourier transform infrared (FTIR) spectra were recorded for these sol−gel-prepared glasses using a Perkin-Elmer 560 double beam IR spectrometer (resolution = 1 cm^{-1}) in the frequency range 4000−400 cm^{-1}. FTIR measurements were made using KBr pellets containing 1 wt % of powdered glass. Spectral grade KBr was used for the preparation of pellets. The IR spectra of the samples were recorded at room temperature.

^{29}Si (59.6 MHz) and ^{31}P (121.4 MHz) HR MAS NMR spectra of the samples were recorded using a Bruker MSL-300 solid-state high-resolution spectrometer. Spinning rates of 3.5 and 5 kHz were employed for recording ^{31}P and ^{29}Si spectra, respectively. The sidebands were identified by their drift when the spectra were recorded at different spinning rates.

Conductivity Measurements. The samples were ground-pressed into circular disks of 1 cm diameter and 0.2 cm thickness and were used for conductivity measurements. The two parallel faces of the disks were coated with silver paint for use as electrodes. Conductance (G) and capacitance (C) were measured using an HP impedance analyzer (model HP 4192 A) in the frequency range from 10 Hz to 1 MHz at various temperatures from 300 to 773 K. The temperature of the sample was measured using a chromel−alumel thermocouple. The temperature was controlled using a Heatcon temperature controller with an accuracy of ±1 K.

Data Analysis. The real (Z') and imaginary (Z'') parts of the complex impedance (Z^*) were obtained from the measured conductance and the capacitance using the relations

$$Z' = G/(G^2 + \omega^2C^2) \quad \text{and} \quad Z'' = \omega C/(G^2 + \omega^2C^2) \quad (1)$$

where, G is conductance, C is parallel capacitance, and ω is the angular frequency. The real (ϵ') and imaginary (ϵ'') parts of the complex dielectric constant were calculated from the relations

$$\epsilon' = Cd/\epsilon_o A \quad \text{and} \quad \epsilon'' = \sigma/\omega\epsilon_o \quad (2)$$

where d is the sample thickness, A is the cross-sectional area, σ is the conductivity, and ϵ_o is the permittivity of free space.

The data were also analyzed using the electrical modulus formalism. The real (M') and imaginary (M'') parts of the complex electrical modulus ($M^* = 1/\epsilon^*$) were obtained from ϵ' and ϵ'' values

$$M' = \epsilon'/((\epsilon')^2 + (\epsilon'')^2) \quad \text{and} \quad M'' = \epsilon''/((\epsilon')^2 + (\epsilon'')^2) \quad (3)$$

Results and Discussion

The compositions and sample designations are given in Table 1. The behavior of gels at the end of various hold temperatures (varying between 2 and 6 h) is also indicated in Table 1. The absence of a peak in the X-ray diffractograms confirmed the amorphous nature of the sample. It was not possible to observe the glass transition in any of the glasses. The glass transitions in silica and silica-rich glasses are generally very difficult to identify in thermograms. A similar observation has been reported for the lithium silicophosphate system of glasses in the literature.[22,24] Further phase separation and crystallization of the silicophosphates may occur at temperatures lower than the glass transition temperature, T_g. The samples with the codes CP4, CP5, and CL5 were found to form as mixtures of amorphous and crystalline phases and were unsuitable for the present investigations. It may also be noted that the samples CP3, CL1, CL4, and CS1 indicated formation of crystallites attributable to LiH_2PO_4 below 523 K, but the crystalline features in XRD disappeared around 523 K and they formed glasses above this temperature without any attendant endotherms attributable to melting. The glasses used in further investigations are marked in Table 2. The typical variation of XRD patterns at various stages of heat treatment is shown in Figure 1 for the case of CP3 glass.

Table 1. Crystalline/Amorphous Behavior of Lithium Silicophosphate Xerogels

composition				behavior at various temperatures[a]				
Li_2O	SiO_2	P_2O_5	glass designation	373 °C	473 °C	573 °C	673 °C	773 °C
10	70	20	CP1	A	A	A	A	A
15	65	20	CP2	A	A	A	A	A
20	60	20	CP3	C+A	C+A	A	A	C+A
25	55	20	CP4	C+A	C+A	C+A	C+A	C+A
30	50	20	CP5	C+A	C+A	C+A	C+A	C+A
20	70	10	CL1	A	A	A	A	C+A
20	65	15	CL2	A	A	A	A	A
20	60	20	CL3	C+A	C+A	A	A	C+A
20	55	25	CL4	C+A	C+A	A	A	C+A
20	50	30	CL5	C+A	C+A	C+A	C+A	C+A
25	70	05	CS1	C+A	C+A	A	A	C+A
20	70	10	CS2	A	A	A	A	C+A
15	70	15	CS3	A	A	A	A	A
10	70	20	CS4	A	A	A	A	A

[a] A, amorphous; C, crystalline. The Peaks could be identified with one or two of the following phosphates, LiH_2PO_4, $Li_3HP_2O_7$, and $LiPO_3$.

Table 2. Density, Molar Volumes, Conductivity (σ_{423K}), Activation Energy for Conduction (E_a), and Activation Energy for Relaxation (E_t)

		molar vol, cm3					
glass code	density, g/cm^3	obsd	calcd	σ_{423K}, S/cm	$E_a \times 10^{-1}$, eV	$E_t \times 10^{-1}$, eV	τ_o, s
CP1	1.27	57.7	45.4	$(2.05 \pm 0.07) \times 10^{-7}$	4.0 ± 0.1	8.0 ± 0.07	7.80×10^{-12}
CP2	1.30	55.2	44.8	$(6.31 \pm 0.05) \times 10^{-9}$	6.4 ± 0.08	6.4 ± 0.09	1.68×10^{-13}
CP3	1.35	52.1	44.1	$(6.12 \pm 0.06) \times 10^{-9}$	6.9 ± 0.09		
CL1	1.67	37.2	34.5	$(1.03 \pm 0.06) \times 10^{-7}$	7.1 ± 0.07	7.8 ± 0.07	6.50×10^{-13}
CL2	1.43	46.4	39.3	$(4.08 \pm 0.06) \times 10^{-8}$	7.0 ± 0.08	8.0 ± 0.07	4.17×10^{-14}
CL4	1.18	62.7	48.9	$(8.00 \pm 0.08) \times 10^{-7}$	4.2 ± 0.1		
CS3	1.61	43.1	39.9	$(2.00 \pm 0.05) \times 10^{-8}$	6.7 ± 0.08	7.7 ± 0.08	5.75×10^{-14}

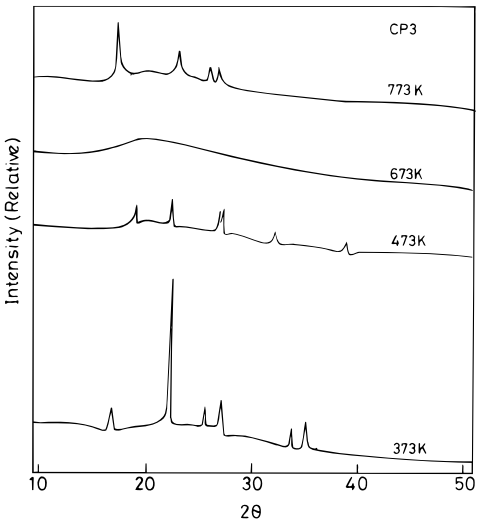

Figure 1. X-ray diffractograms of the sample CP3 at various temperatures.

Density and Molar Volume. The densities of the glasses obtained after heating the various gels at 673 K are given in Table 2. Molar volumes were calculated with the molecular weight corresponding to the weighted sum of the molecular weights of the component oxides. Molar volume estimates were also obtained as simple weighted sums of the molar volumes of fused quartz, glassy P_2O_5, and crystalline Li_2O. These are also listed in Table 2. Since glassy P_2O_5 has the largest molar volume (corresponding to the volume of two connected $POO_{3/2}$ tetrahedra), the molar volume increases to high values as P_2O_5 content increases in the glassy samples. The estimated molar volumes also vary roughly in the same manner in all glassy samples. In glasses such as CL1 and CS2, observed molar volumes are significantly lower, which is expected because of the crystallization of Li_3PO_4, which possesses lower molar volumes. However, in the case of CP1 and CL4, the observed molar volumes are significantly higher and this is suggestive of the presence of uneliminated water in the form of hydroxyl groups. We will see later that this manifests in pronounced protonic conductivities in these samples.

Thermal Studies. The thermograms of various glasses are shown in Figure 2. The enthalpy (ΔH) values of the endotherms are generally low and the estimation of enthalpy value for the glass CP2 is shown in the inset of Figure 2. We suspect that the first endotherm around 400 K corresponds to loss of water adsorbed by the samples during storage. However, the endotherm in the region above 523 K is likely to be caused by the elimination of water by condensation of hydroxyls still retained by the glass structure, and this aspect will be discussed in a later section. It is, however, important to note that there is no exotherm that can be attributed to any crystallization in the samples. No attempt was made to analyze the kinetics of the processes associated with the endotherms.

Infrared Spectra. The IR spectra of the glasses recorded between 4000 and 400 cm^{-1} are presented together in Figure 3. The frequencies of the major absorption peaks are also listed in Table 3. Assignments of these frequencies have been done on the basis of literature reports[26−29] and are also indicated in Table 3. We note that there are broad and fairly intense absorption peaks around 3400 and 1650 cm^{-1} in all the

(26) Zarzychi, J.; Nandin, F. *J. Chim. Phys.* **1961**, *58*, 830.
(27) Chakraborty, I. N.; Condrate, R. A., Sr. *Phys. Chem. Glasses* **1985**, *26*, 68.
(28) Kamiya, K.; Sakka, S. *Res. Rep. Fac. Eng. Mie. Univ.* **1977**, *2*, 87.
(29) Corbridge, D. E. C.; Lowe, E. J. *J. Chem. Soc.* **1954**, 493.

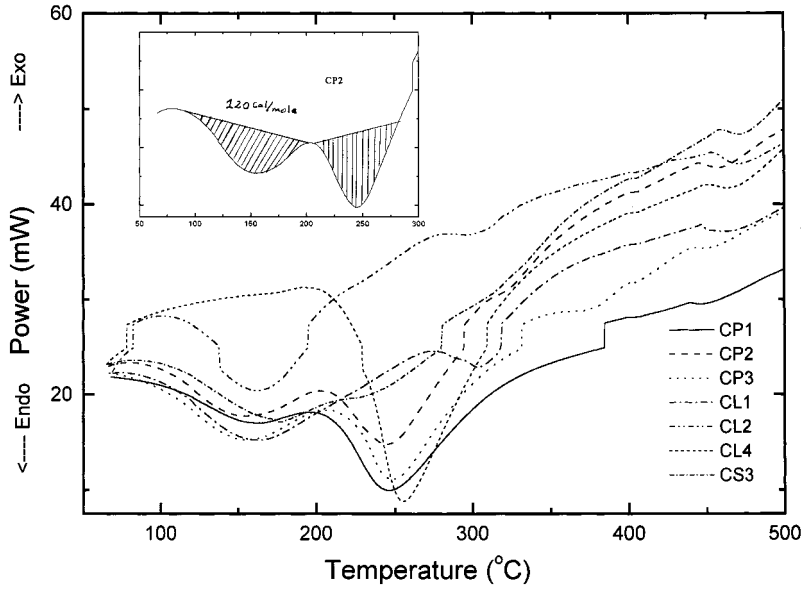

Figure 2. DTA thermograms of silicophosphate glasses of varying compositions.

Table 3. FTIR Absorption Bands for the Lithium Silicophosphate Glasses of Varying Compositions

glass code	absorption bands (cm^{-1})							
CP1	3436	2400	1660	1186	1093	979	803	478
CP2	3431	2400	1667	1207	1093	974	803	478
CP3	3434	2400	1662	1233	1093	969	803	472
CL1	3443	2400	1660	1230	1098	962	803	483
CL2	3446		1660	1207	1098	960	803	468
CL4	3400		1660	1217	1098	970	803	473
CS3	3444		1660	1230	1093	960	803	475
assingments	Si−OH stretching	P−OH stretching	Si−OH deformation	P═O stretching	Si O_4 & PO_4 tetrahedra	Si−O−P linkages	Si−O−Si bending mode	O−Si−O bending mode

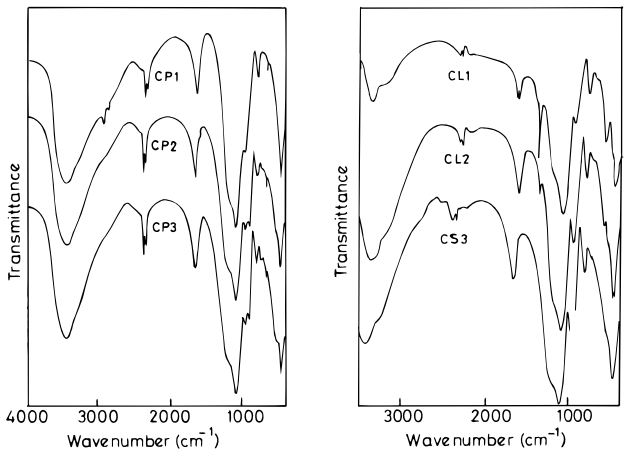

Figure 3. FTIR spectra of silicophosphate glasses of varying compositions.

glasses, although their intensities are different in different glasses. It may be seen that these peaks appear together and with another peak around 2400 cm^{-1}. The intensities of these peaks can be seen to vary directly with the ratio $R = Li_2O/P_2O_5$. In fact, when $R \geq 1$ in the glass, the 2400 cm^{-1} is almost completely eliminated, although the 3400 and 1650 cm^{-1} combination remains. We associate this combination of peaks to the presence of OH groups attached to Si and the two bands to Si−OH stretching (3400 cm^{-1}) and Si−OH deformation (1650 cm^{-1}) bands.[26] The 2400 cm^{-1} (fairly sharp) band is associated with the P−OH stretching.[26] The absorption in the region of 1200 cm^{-1} (mostly appearing as an intense shoulder) is ascribed to P═O stretching of the phosphate units.[29] In the region of ~1100 cm^{-1}, the absorptions are due to the stretching modes of both PO_4 and SiO_4 tetrahedra.[27] The prominent shoulder around 970 cm^{-1} can be ascribed to Si−O−P linkages, while the 800 cm^{-1} sharp peak can be associated with the Si−O−Si bending in the glass structure.[26] The intensity of the 800 cm^{-1} absorption is relatively unaffected because all the glass compositions contain much higher percentage of SiO_2 than P_2O_5. At the farther end of the IR spectra, there is a fairly sharp peak at 480 cm^{-1}, which is ascribed to O−Si−O bending modes,[28] and for the reasons just stated, the intensity of this peak remains high in all the compositions. No specific feature in the IR absorption spectra could be ascribed to Li ion cage vibrations, although in the literature the 400−450 cm^{-1} absorption is ascribed to it.[30]

NMR Spectra. The high-resolution MAS NMR spectra of the glasses are presented in parts a and b of Figure 4 for ^{29}Si and ^{31}P nuclei, respectively. The chemical shifts for various resonances are listed in Table 4. The resonances are grouped according to the values (within a range) of chemical shifts. The ^{31}P resonance peaks were generally sharp (fwhm is 5 ppm or less) and only in the cases of CL2 and CL4 were the fwhm values higher than 10 ppm. In comparison, ^{29}Si resonances were broad (fwhm varying between 12.5 and 20 ppm).

(30) Exarhos, G. J.; Miller, P. J.; Risen, W. M., Jr. *J. Chem. Phys.* **1974**, *60*, 4145.

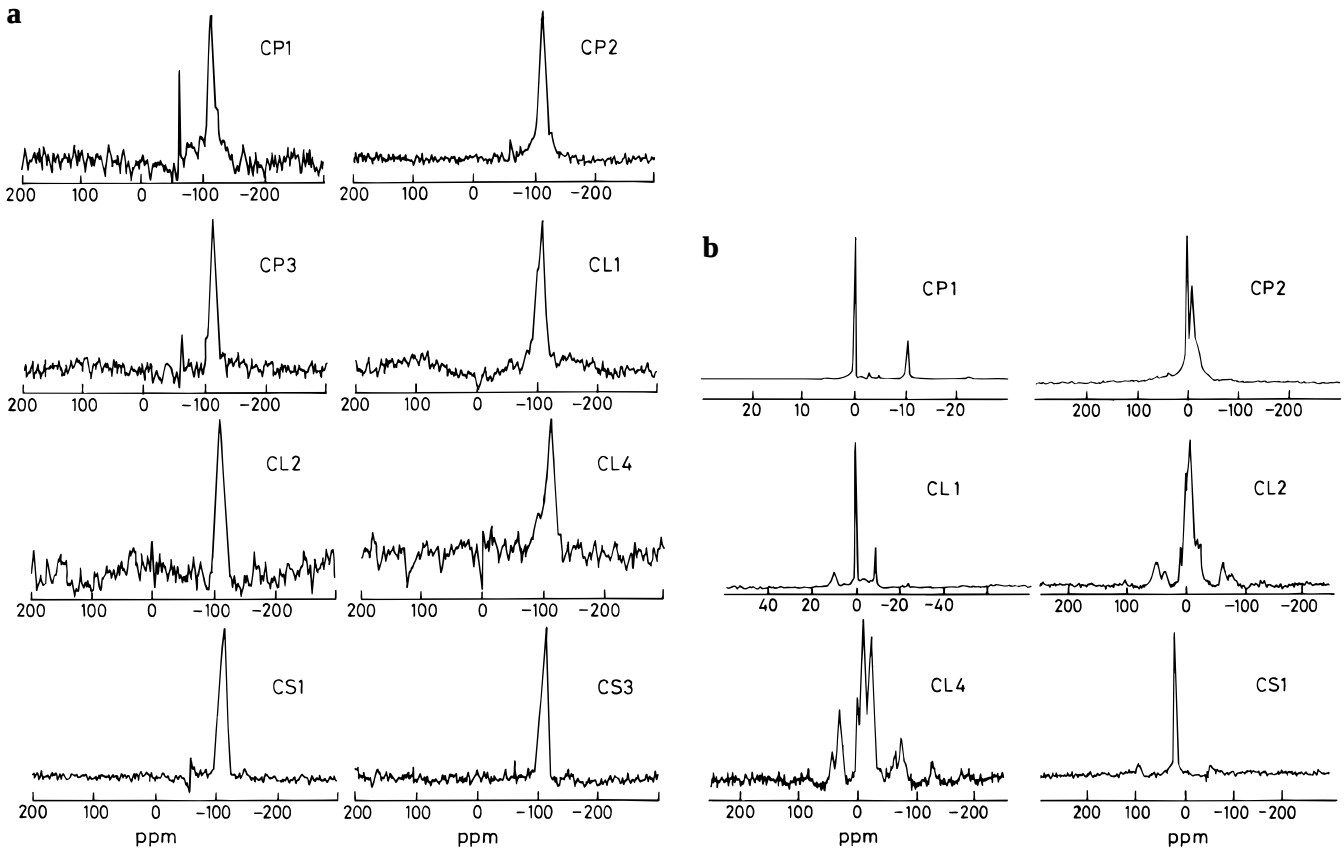

Figure 4. (a) ^{29}Si MAS NMR spectra of silicophosphate glasses of varying compositions; (b) ^{31}P MAS NMR spectra of silicophosphate glasses of varying compositions. The star symbol represents the sideband.

Table 4. Chemical Shifts and fwhm for the Lithium Silicophosphate Glasses of Varying Compositions

	^{31}P NMR resonance				^{29}Si NMR resonance	
sample code	δ of P1	δ of P2	δ of P3	fwhm	δ	fwhm
CP1		0.0	−10.3	4.17 (P2)	−114.6	15.0
CP2		0.03	−9.71	5.72 (P2)	−111.9	13.1
CP3					−112.2	12.5
CL1	10.0	0.65	−10.1	0.49 (P3)	−110.3	16.3
CL2	12.1	0.56	−8.1	13.9 (P3)	−110.3	13.1
CL3		0.0	−12.5	11.3 (P3)	−112.2	12.5
CL4					−113.3	19.7
CS1	12.2			2.82 (P1)	−111.0	15.0
CS3					−111.7	14.4

^{31}P resonances belong to three groups corresponding to the chemical shift values −8 to − 12.5, 0.0−0.6, and 10−12.1 ppm. These have been tentatively associated with phosphatic species P_3, P_2 and P_1, respectively, as shown in Table 4 and they correspond to

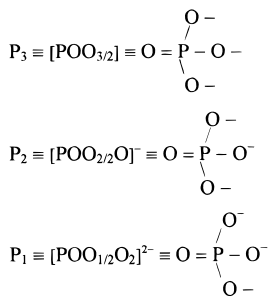

It may be noted that P_3, P_2, and P_1 are actually neutral, singly charged, and doubly charged species, respectively, produced by modification of the glass by the presence of Li_2O. P_2 and P_1 are the meta- and pyrophosphate species. It is seen that no signals attributable to orthophosphate were observed in the NMR spectra. However, the resonances occur at values that suggest a significant positive shift of each group of resonances.[31] Since these glasses are made with a high ratio of SiO_2/P_2O_5, the phosphate groups are isolated by the silicate units, which are also covalently bonded to the phosphates. This can give rise to significantly different electron densities in the valence shell of phosphorus in glass compared to the phosphorus in the orthophosphoric acid solution used as reference.

^{29}Si NMR of the glasses gave rise to single resonance in the range from −110 to −115 ppm. This resonance is generally associated with ($SiO_{4/2}$) units, which are designated as ϕ_4, where 4 is the number of bridging oxygens present in the coordination of Si (denoted as ϕ). Although it is surprising at first sight that only ϕ_4 is present in all the compositions, we will see later that

(31) Prabakar, S.; Rao, K. J.; Rao, C. N. R. *Chem. Phys. Lett.* **1977**, *139*, 96.

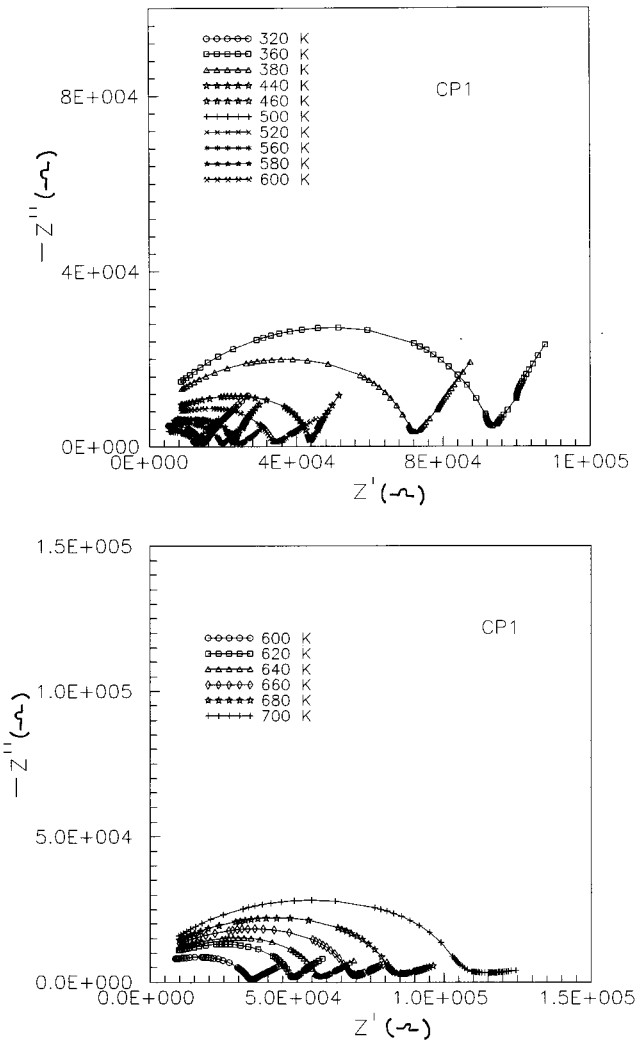

Figure 5. Complex impedance plots of CP1 glass at various temperatures.

this is totally consistent with the chemistry of these silicophosphate glasses.

Composition Dependence of Dc Conductivity. The dc resistances of all the samples were obtained from the impedance analysis. Figure 5 shows a typical complex impedance plot for the glass CP1 at various temperatures. The spikelike trend in Figure 5 represents the electrode effects, whereas the semicircular arc is associated with the parallel combination of bulk resistance and bulk capacitance of the sample. Also, the semicircular arcs were found to be depressed and the centers of these circles lie below the positive real axis, which suggests that the associated relaxations are not Debye-like but conform to a distribution of relaxation times. The dc resistances of the samples were obtained by nonlinear least squares (NLLS) fitting of the impedance data using the Boukamp software package.[32] The intercept of the impedance on the *x*-axis gives the dc resistance of the sample. It is seen from Figure 5 that as the temperature increases the intercepts shift toward higher frequencies because of the decrease in resistance due to the thermally activated

(32) Boukamp, B. A. *Equivalent Circuit Users Manual*, University of Twente: Twente, 1989.

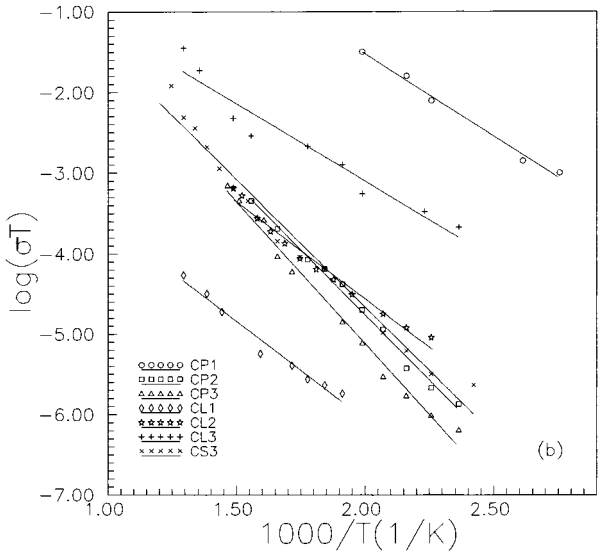

Figure 6. Arrhenius plots (above 400 K) of silicophosphate glasses of varying compositions.

nature of the conduction process. The conductivities of all the samples were calculated at different temperatures using the dc resistance and sample dimensions.

The temperature dependences of dc conductivities are shown in Figure 6 in the form of Arrhenius plots. At lower temperatures (300−400 K) the conductivities were found to decrease with increasing temperature (not shown in Figure 6), which is indicative of instabilities which we associate with the loss of adsorbed water. A similar conductivity trend has been observed by Hayri et al. in this system.[22] However, in the high-temperature regime, above 400 K the conductivity behavior was quite stable and reproducible. As shown in Figure 6, the conductivities above 400 K increase with temperature, which is typical of ionically conducting glasses. The activation energies for the Li ion motion is obtained by least-squares fitting of the conductivity data (above 400 K) shown in Figure 6 b to the equation

$$\sigma = \sigma_o \exp(-E_a/kT) \qquad (4)$$

where σ_o is the preexponential factor and E_a is the activation energy for conductivity. Table 2 lists the conductivities at 423 K and the activation energies for conductivity.

Conductivities generally range from 10^{-7} to 10^{-9} S cm^{-1}, and the activation barriers vary from 0.4 to 0.7 eV. But if the E_a of the two compositions CP1 and CL4, which exhibit particularly low values of activation barrier, are excluded, the range of values of E_a is rather narrower (0.64−0.71 eV). It will be seen that the behavior of ac conductivity of the CP1 and CL4 samples is also different. We suspect that the low activation barriers and high conductivities of the samples are due to transport of protons and not Li^+ ions. It may be noted that in these two glasses, the IR bands at around 3400 and 1660 cm^{-1} attributed to OH groups is notably stronger than in other glasses. We will show later that the protons may not be from OH groups attached to phosphorus, because their concentration is much lower (see the 2400 cm^{-1} peak in Figure 3). In Figure 7a, the variation of the conductivities at 423 K and activation

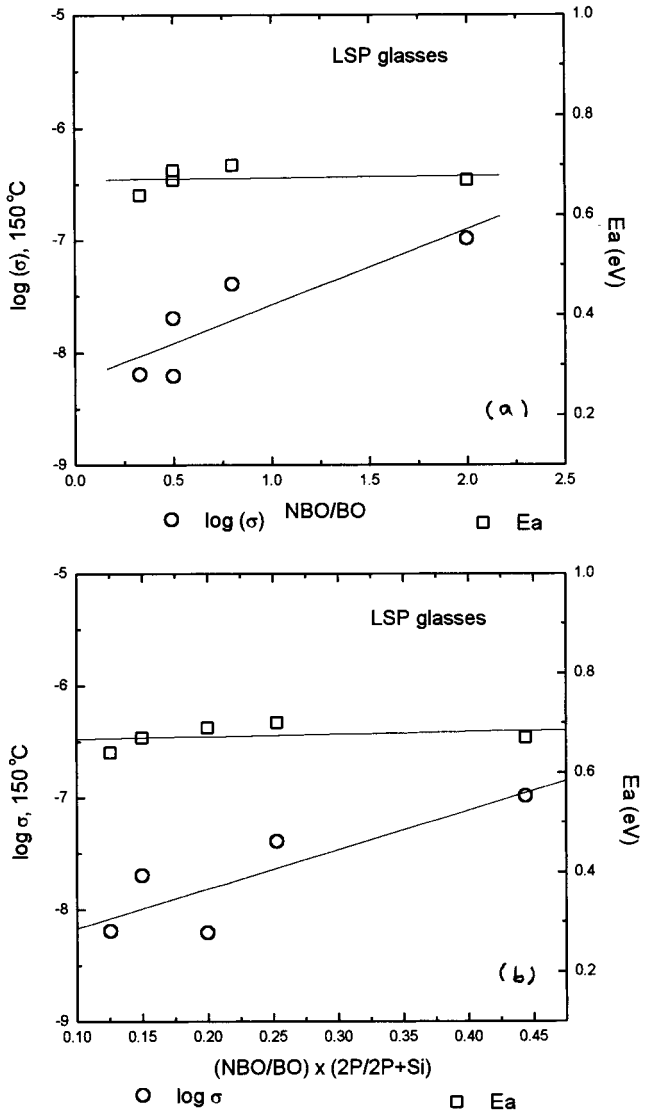

Figure 7. Variation of dc conductivity at 423 K and activation energy, E_a, as a function of NBO/NBO ratio (a) without dilution effect and (b) with dilution effect.

barriers have been plotted as a function of the ratio of nonbridging oxygen to bridging oxygens (NBO/BO). There is generally an increasing trend for both the activation energy and conductivity as a function of the ratio of NBO/BO (same as the Li_2O concentration to $2P_2 + P_1$). In this plot, however, the two rather highly conducting samples CP1 and CL4 have not been included, as their conductivities are likely to be protonic.

Ac Conductivity Behavior. The frequency variation of ac conductivities for the various compositions are given in Figure 8 at various temperatures. It is seen that the flat (frequency independent) part of the conductivity was observed only at rather high temperatures. We may note here that the analysis of ac conductivity measurements were done only for data above 400 K, because of the problem of adsorbed water, as noted earlier in the dc conductivity section. The conductivity variation with frequencies has been fitted to the Almond−West type of equation[33,34] by nonlinear regression analysis

$$\sigma(\omega) = \sigma(0) + A\omega^s \qquad (5)$$

Table 5. Conductivity at Zero Frequency, σ_0, Ac Conductivity Prefactor, *A*, Power Law Exponent, *s*,[a] and $T_{s_{min}}$ and the KWW Stretching Constant, β

glass code	$\sigma(0)$, S/cm	A, S/cm	s_{min}	$T_{s_{min}}$, K	β
CP1	5.35×10^{-5}	2.35×10^{-9}			
CP2	1.25×10^{-7}	1.12×10^{-9}	0.46	563	0.40
CP3	6.81×10^{-9}	3.67×10^{-10}	0.43	503	0.44
CL1	1.17×10^{-9}	4.27×10^{-10}	0.50	563	0.34
CL2	6.55×10^{-8}	1.75×10^{-9}	0.45	553	0.36
CL4	2.48×10^{-6}	2.99×10^{-9}	0.54	503	
CS1	9.47×10^{-8}	1.11×10^{-9}	0.48	543	0.36

[a] *s* was determined by fitting the conductivity data to the equation $\sigma(\omega) = \sigma(0) + A\omega^s$.

where $\sigma(0)$ is the zero frequency conductivity, A is a constant, and s is the power law exponent, which was found to be temperature dependent. The various parameters determined in this manner for the different compositions at 423 K are listed in Table 5. $\sigma(0)$ values are in the range of 10^{-9}−10^{-10} S/cm, which is significantly lower than the dc conductivities estimated from the impedance plots. This clearly shows that $\sigma(0)$ obtained from ac measurements and σ from σ_{dc} measurements are rather different quantities and associated with entirely different mechanisms of transport.[35] The conductivity behavior has been examined at various temperatures. It is found that in all the cases, s is temperature dependent and exhibits a minimum. The variation of s with temperature is shown in Figure 9. The values of s are typically in the range of 0.43−0.65. In all the cases, a minimum in s is observed which is significantly low (see Table 5). Observation of the minimum in s as a function of temperature can be directly related to the existence of a range of relaxation parameters and mechanisms. The observed s in these cases, which is a consequence of fitting the data to a power law, represents only a combined effect. It is intuitively obvious that the various relaxational pathways are characterized by different s values. Therefore, the magnitude of contribution to the measured ac conductivity by the particular polarization mode varies with temperature and becomes dominant at particular temperatures.

Such temperature dependences and occurrence of minima in measured s values have been reported in the literature.[36−38] Jain et al. first reported such systematic studies of the frequency dependence of conductivity and the temperature dependence of the power law exponent in rubidium−germanate, sodium−rubidium−germanate, fluorine-doped sodium−triborate, and a fluorine-doped mixed lithium−sodium−triborate glasses.[36] In their study they clearly pointed out that the frequency power law exponent s does depend very much on temperature and showed that it exhibits a shallow minimum in the s verses temperature plot and they argued that the temperature independent trend of s, as suggested by Almond and West,[33,34] is invalid. Elliott reinvestigated[37]

(33) Almond, D. P.; West, A. R.; Grant, R. J. *Solid State Commun.* **1982**, *44*, 1277.
(34) Almond, D. P.; Duncan, G. K.; West, A. R. *Solid State Ionics* **1983**, *8*, 159.
(35) Elliott, S. R.; Henn, F. E. G. *J. Non-Cryst. Solids* **1990**, *116*, 179.
(36) Jain, H.; Mundy, J. N. *J. Non-Cryst. Solids* **1987**, *91*, 315.
(37) Elliott, S. R. *Solid State Ionics* **1988**, *27*, 131.
(38) Verhoef, A. H.; den Hartog, H. W. *Solid State Ionics* **1994**, *68*, 305.

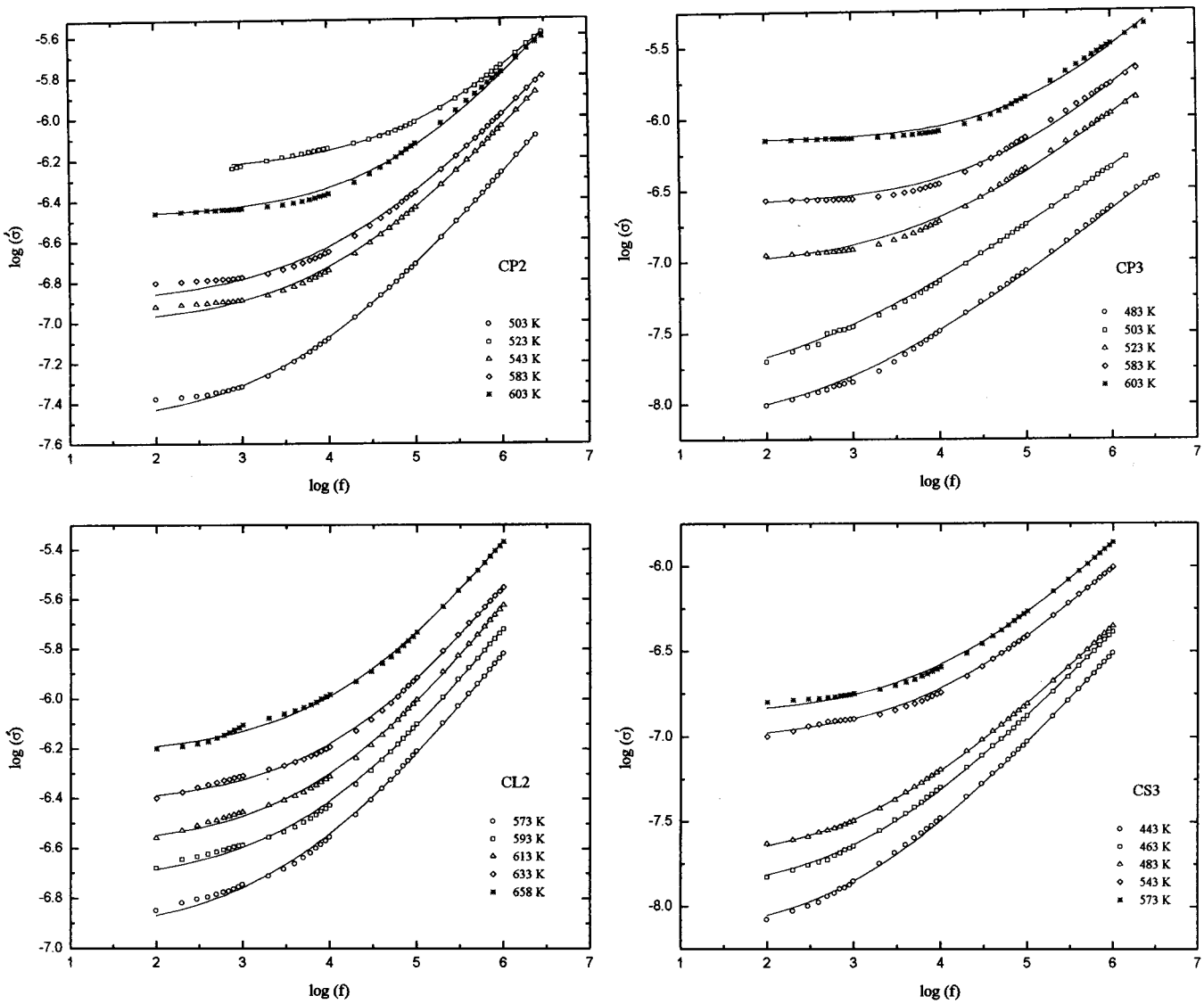

Figure 8. log(σ') versus log(f) plots for few silicophosphate glasses. The continuous line represents the fit of conductivity data the equation $\sigma(\omega) = \sigma_0 + A\omega^s$.

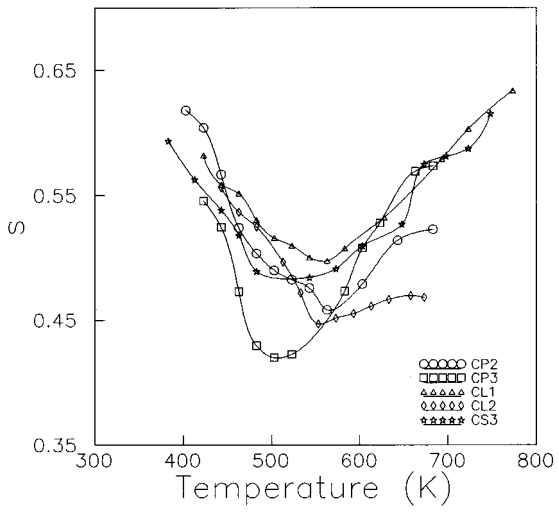

Figure 9. Variation of power law exponent, s, as a function of temperature for various silicophosphate glasses.

the results reported by Jain et al. and found that it is possible to understand the temperature dependence of s using the overlapping large polaron (OLP) model.[39,40]

Verhoef et al. have also reported a detailed study on the temperature dependence of s in lithium borate and Li_2Cl_2-doped lithium borate glasses.[38] Even though Verhoef et al. observed that s decreases with increasing temperature, they did not observe a well-defined minimum in s. They have also reported a composition dependence of the $T_{s_{min}}$ and magnitude of s_{min}. They concluded that a lower minimum value of s could be linked to a higher rate of successful jumps and thus higher dc conductivity. The occurrence of minima in lithium thioborate glasses was earlier examined[41] on the basis of Elliott's diffusion-controlled relaxation (DCR) model.[35,42] The principal result of DCR is that the relaxation function $\phi(t)$ can be expressed as

$$\phi(t) = \exp[(-t/\tau_1)^{1/2}] \exp[-t/\tau] \qquad (6)$$

where τ_1 is the effective relaxation time equal to $\pi l_0^2/$

(39) Long, A. R. *Adv. Phys.* **1982**, *31*, 553.
(40) Long, A. R.; Balkan, N.; Hogg, W. R.; Ferrier, R. P. *Philos. Magn.* **1982**, *B45*, 497.
(41) Rao, K. J.; Estournes, C.; Menetrier, M.; Levasseur, A. *Philos. Magn.* **1994**, *B70*, 809.
(42) Elliott, S. R.; Owens, A. P. *Philos. Magn.* **1989**, *B60*, 777.

$4D$, where l_0 is a characteristic jump distance and D is the diffusion coefficient. Equation 6 makes the assumption that the conducting ion, namely Li^+, jumps between (local) equivalent positions whereby it contributes to the polarization current with a probability $P(t)$ so that $1 - P(t)$, which is the probability that it does not diffuse, is given by $\exp[(-t/\tau_1)^{1/2}]$ according to Glarum−Bordewjick analysis. It has been shown elsewhere[41] that a formally identical expression is obtained using a vacancy model. Stretching of the relaxation time occurs by sudden cessation of the relaxation process associated with ion-vacancy jumps when a vagrant Li^+ ion arrives suddenly at the vacancy. Both DCR and vacancy models, therefore, lead to the same operative expressions. With the assumption[35,42] that relaxation data can be force fit into Davidson−Cole type of expression, it is possible to write s as

$$s = [\pi\tau/4\tau_1]^{1/2} = (D\tau/l_0^2)^{1/2} \tag{7}$$

where τ is the relaxation time characterizing the jump of Li^+ ions between two equivalent positions as in the (Li^+−vacancy couple) and is given by

$$\tau = \tau_0 \exp(W/kT) \tag{8}$$

where W is the barrier for the local jump motion (diffusion independent). It is evaluated from the temperature dependence of dielectric loss peak. Since D in eq 7 is itself temperature dependent and is given by

$$D = aT\sigma_{dc} = aT\sigma_0 \exp(-E_a/kT) \tag{9}$$

where E_a is the activation barrier determined from dc (diffusion dependent) conductivity measurements, $a = k/(ce^2)$, and k, e, and c are Boltzmann's constant, electronic charge, and concentration of charge carriers, respectively. Substitution of eqs 8 and 9 into eq 7 gives

$$s = T^{1/2}b \exp[(W - E_a)/2kT] \tag{10}$$

where $b = (a\sigma_0\tau_0/l_0^2)^{1/2}$. It is evident from the functional form of the eq 10 that s should exhibit a minimum when $W - E_a = kT$.

We examine the present observation of s_{min} in silicophosphate glasses in the light of the above expression for the case of CS3. An expression for s_{min} is obtained by setting $ds/dT = 0$ in eq 10, and then we obtain $b = s_{min}/(T_{min}^{1/2}e^{1/2})$. Substituting s_{min} and T_{min} listed in Table 5, b is found to be 11.57×10^{-3} $K^{-1/2}$. The concentration of Li^+ ions is obtained from the data in Table 2 as $(\rho/M)2xN$, where ρ is the density, N is Avogadro's number, M is the molecular weight, and x the mole fraction of Li_2O. This has a value of $3.28 \times 10^{28}/m^3$. l_0 is estimated from $(M/2xN\rho)^{1/3}$ and is 5.67×10^{-10} m. σ_0 has been estimated from extrapolation of dc conductivities to the high-temperature limit in Figure 6b and found to be 8.5×10^3 S/cm. Substituting these quantities into the expression for b we get a value of $\tau_0 = 3.114 \times 10^{-13}$ s. This compares very well with the τ_0 values obtained from modulus peaks, given in Table 2 (see later). Further, $1/c\tau_0 = 107$ cm^{-1}, is in reasonably good agreement with the known cage vibrational frequency of Li ions[43] in oxide matrixes which is ≈400 cm^{-1}. We may note here that the equation for τ_0 is rooted in the assumption $s = 1 - \beta$, where β is the Cole−Davidson exponent in relaxation expressions. We will see later that β obtained from dielectric modulus plots is not in conformity with the above assumption; $\beta \neq 1 - s$. Despite this, the fact that there is a reasonable agreement between calculated attempt frequency, $\nu_o(=\tau_0 - 1)$ and the cage vibrational frequency justifies the present approach to rationalize the occurrence of s_{min}. Equation 7, which relates s to the diffusion coefficient and the short-range relaxation times, is of crucial importance for providing the theoretical basis for s_{min}. These two quantities, D and τ, represent the long-range diffusive and short-range (correlated) hopping processes. The latter is a localized process and the associated relaxation is Debye-like and can be interrupted by the unexpected (random) arrival of a second ion at the site, which occurs by diffusion. It is only when the diffusion coefficient varies with temperature at a rate which is exactly the inverse of τ that s can be expected to be a constant. It can be seen from eqs 7 and 8 that it is unlikely to happen. It is interesting to note that low values of s result from a combination of low diffusion coefficient and short relaxation times combined with larger values of the hopping distance, as seen from eq 7. Thus, it is difficult to associate high conductivity per se with low values of s.[38]

The temperature dependence of the ac conductivity has been examined in the light of Kahnt's approach[44] by plotting $\log(\sigma/\sigma_{dc})$ versus $\log(f/f_o)$, where f_o is the relaxation peak frequency obtained from modulus plots (see the later discussion). It is seen from Figure 10 that the superimposability of $\log(\sigma/\sigma_{dc})$ versus $\log(f/f_o)$ measured at various temperatures is not satisfactory, suggesting that the ion transport in these glasses is affected by both structural aspects and ion concentrations.

Electrical Modulus Studies. Relaxation behavior has also been examined using the electrical modulus formalism. The M'' data is fitted to the well-known Kohlraush−William−Watts (KWW) expression[45,46] for stretched relaxation times,

$$\phi(t) = \exp[-(t/\tau)^{\beta}] \qquad 0 < \beta < 1 \tag{11}$$

where β is the stretching constant, t is time, and τ is the relaxation time. The complex electrical modulus, M^*, can be expressed as the Fourier transform of the time derivative of the decay function ϕ(t),

$$M^*(\omega) = M_s[1 - \int \exp(-i\omega t)\{d\phi(t)/dt\}dt] \tag{12}$$

where M_s is the high-frequency limit of the real part of the electrical modulus.

The modulus spectra shown in Figure 11 is typical of glassy state relaxation, and the peak frequency in the imaginary part of the modulus spectra, M'', corresponds to the relaxation frequency, ω_p. It is evident from Figure 11 that the frequency of the relaxation peak shifts toward higher frequency as the temperature

(43) Tarte, P. *Spectrochem. Acta* **1964**, *20*, 238; **1965**, *21*, 313; **1970**, *26a*, 747.
(44) Kahnt, H. *Ber. Bunsen-Ges. Phys. Chem.* **1991**, *95*, 1021.
(45) Kohlrausch, R. *Ann. Phys.* **1847**, *12*, 393.
(46) Williams, G.; Watts, D. C. *Trans. Faraday, Soc.* **1970**, *66*, 80.

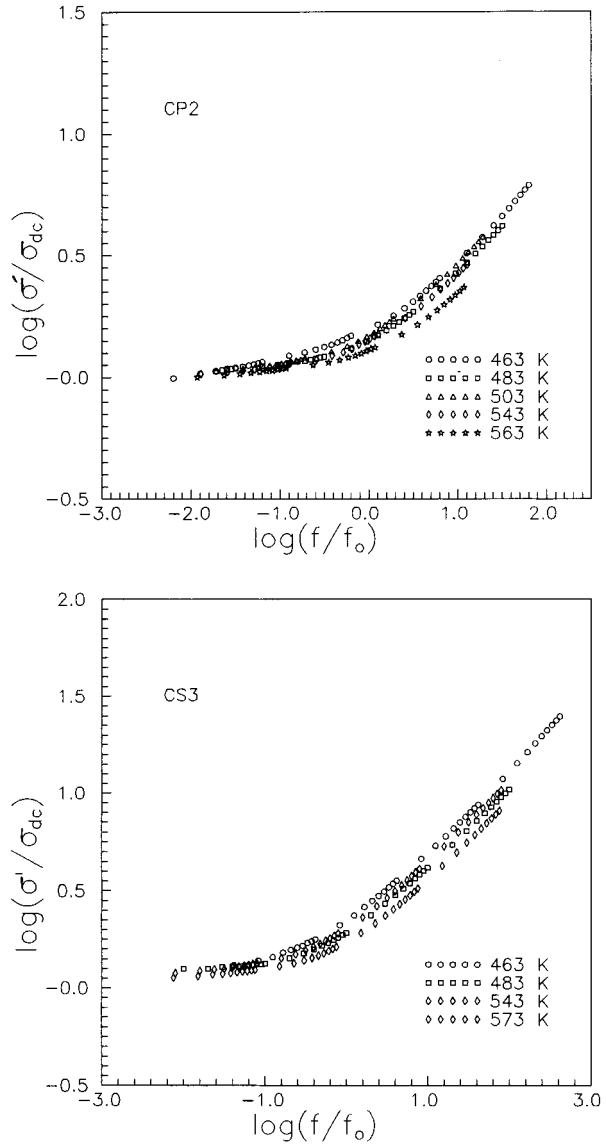

Figure 10. $\log(\sigma'/\sigma_{dc})$ versus $\log(f/f_o)$ for CP2 and CS3 glasses.

increases. The modulus fitting for each composition is performed using the procedure of Moynihan et al.[47] A least-squares iterative routine was developed in C^{++} programming language to fit the experimental data to eq 12 through the decay function $\phi(t)$ (eq 11). The initial values of the free parameters for the fitting, M_s, τ, and β were taken from the high-frequency limit of the real part of the modulus, M', the inverse of the peak frequency, and the fwhm of the relaxation peak, respectively. The continuous lines in Figure 11 represent the fitted values of the M'', whereas the symbols correspond to the experimental data. The agreement between the experimental data and the fitted curve is very satisfactory in Figure 11.

Figure 12 shows the Arrhenius plots of relaxation times for selected glasses. The activation energies for relaxation, E_τ, are obtained from the slopes in Figure 12 and are listed in Table 2, along with the activation energy for dc conductivity. It is evident from Table 2 that the activation energies from relaxation data are slightly higher than those from dc conductivity data.

The stretching exponent β values obtained from the fitting are plotted as a function of temperature for each glass and is shown in Figure 13. It is found that the β values belong roughly to two groups: those (CP2 and CP3) in which the lower bound of β is $\approx$0.4 and those (CL1, CL2, and CS3) in which the upper bound of β is $\approx$0.4. There is significant scatter of β values at some temperatures (for CP2 and CP3) for which there is no clear explanation, but it may be due to inadequacies in the frequency window. The uncertainties in β values in general is low and is indicated in Figure 13. It is interesting to note that in the first category ($\beta > 0.4$), β is relatively independent of temperature, while in the second category, β values tend to exhibit maxima. Toward high temperatures (>600 K), β values decrease to <0.25, suggesting that β values may approach 0. Hence, a temperature independent loss regime may exist at still higher temperatures. Perhaps, this is the first time that a temperature-dependent maximum in β has been observed in glasses. Another surprising feature is the low magnitude of β, although the compositions of glasses are rich in silica and the average inter-Li ion distances are almost close to 6 Å. This may actually be related to the fact that Li^+ ions are all present in the vicinity of the phosphate chains, thereby reducing the volume effectively used by Li^+ ions for conduction. Thus the inter-Li^+ ion distances are reduced. A positive correlation among inter-Li^+ distances, dc activation barriers, and β values has been suggested by Patel et al.[48] and Muthupari et al.[49] By comparison of the activation barriers listed in Table 2 and the β values, we see that such a correlation between dc activation barriers and magnitudes of β is borne out in these glasses. Figure 14 shows a reduced plot of $M''/M''(\max)$ vs $\log(f/f_{max})$ for two glasses with typically high and low values of β and measured over a temperature range of 180 K. The superimposability is notably better in the case of CP3, where β itself is temperature independent. We may tentatively ascribe this difference to a plurality of temperature-dependent mechanisms of relaxation, which in turn must be related to the multiplicity of environments of Li^+ ions in the system.

Structural Model of the Glasses. These sol−gel-prepared glasses are rather unusual. They have larger molar volumes than the linear sum of molar volumes of the component oxides (see Table 2), in which the volumes of P_2O_5 and SiO_2 have been taken for their glassy state. The glass structure is, therefore, rather open. The method of preparation involves use of phosphoric acid and TEOS with $LiNO_3$ in solution, and the gelation has been carried out at acidic pH (HNO_3 was added to catalyze the gelation). Since both P_2O_5 and SiO_2 are acidic oxides, acid catalysis is not expected to lead to any microstructural texturing.[50,51] We therefore expect a completely homogeneous sol formation. It is further assumed that phosphoric acid and TEOS establish a preferred environment of each other at the stage of gelation. We treat it as unimportant for our

(47) Moynihan, C. T.; Boesch, L. P.; Laberge, N. L. *Phys. Chem. Glasses* **1973**, *14*, 122.

(48) Patel, H. K.; Martin, S. W. *Phys. Rev.* **1992**, *B45*, 10292.

(49) Muthupari, S.; Lakshmi Raghavan, S.; Rao, K. J. *J. Phys. Chem.* **1996**, *100*, 4243.

(50) Nagarajan, V. S.; Rao, K. J. *J. Solid State Chemistry* **1990**, *88*, 419.

(51) Nagarajan, V. S.; Rao, K. J. *J. Solid State Chemistry* **1991**, *94*, 149.

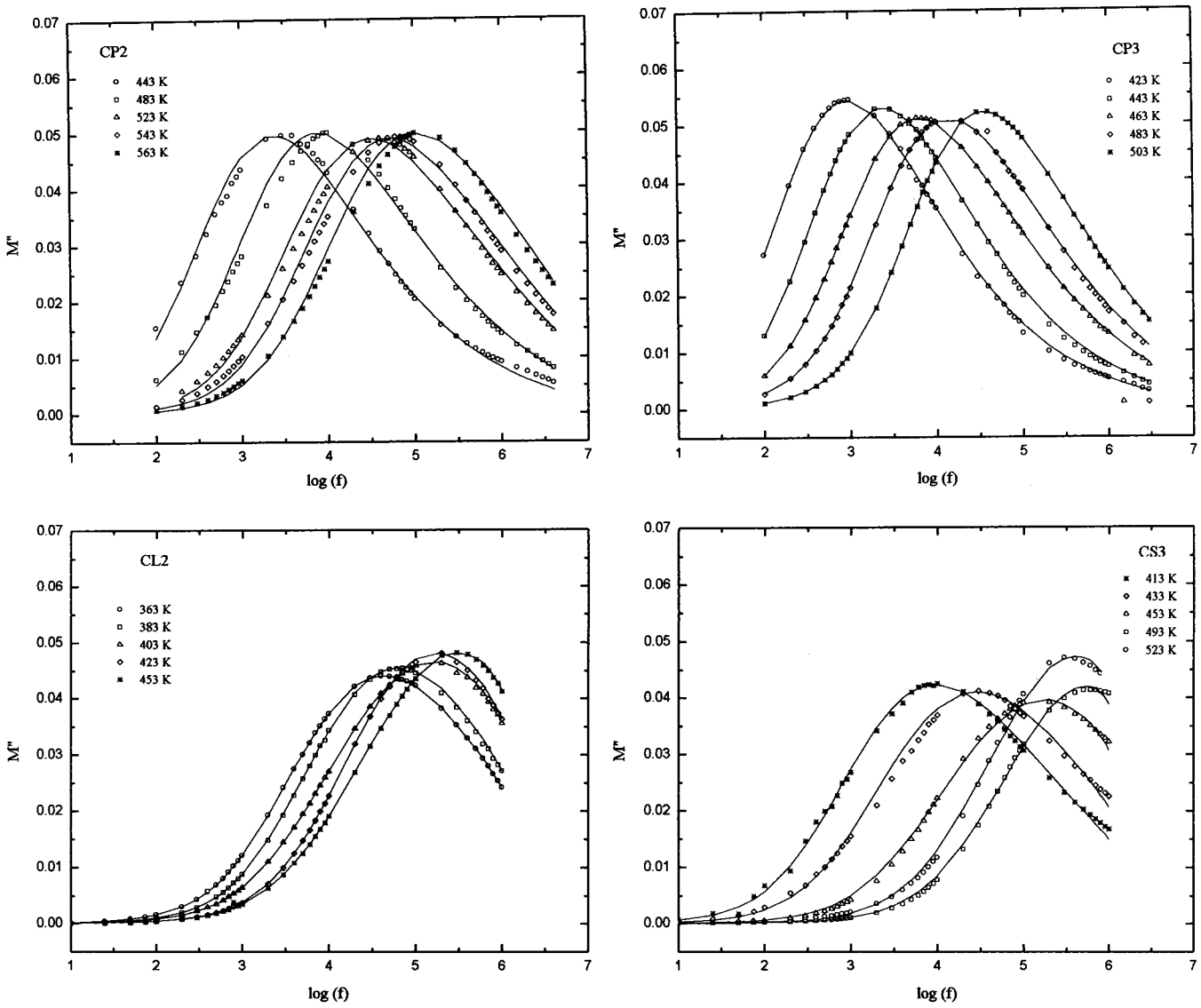

Figure 11. M'' versus log(f) plots for few lithium silicophosphate glasses. The continuous line represents the fit of the modulus data to the decay function $\phi(t) = \exp[-(t/\tau)^{\beta}]$.

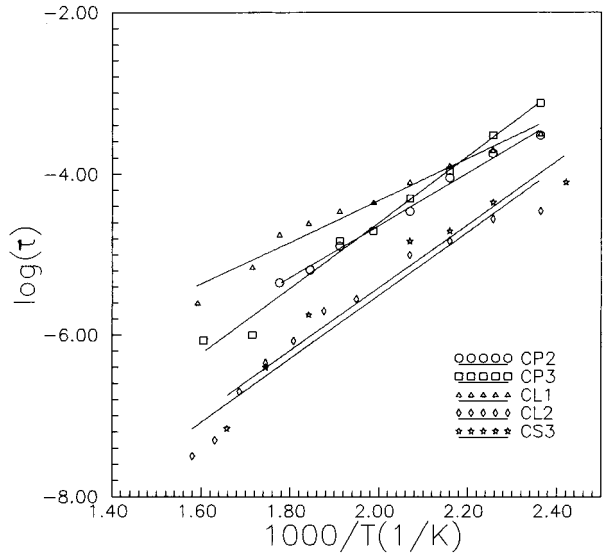

Figure 12. log(τ) versus 1000/T plots of lithium silicophosphate glasses.

purpose whether during gelation Si−O−P bonds are formed directly by elimination of ethyl alcohol or via a second stage at which a condensation occurs between Si−OH and P−OH groups. Si−O−Si bonds, however, may occur through condensation of the latter kind. $LiNO_3$ is homogeneously distributed in the gel. However, when the xerogel is heated to 573 K and cooled, the product obtained is a $Li_2O-SiO_2-P_2O_5$ glass of the appropriate composition. All the nonoxide components are eliminated by evaporation and decomposition.

The structure of such a gel-derived glass is modeled as follows. A binary glass is visualized to be formed with SiO_2 and P_2O_5, which are treated as $SiO_{4/2}$ and $2POO_{3/2}$ groups. On the assumption that $POO_{3/2}$ prefers to coordinate with $SiO_{4/2}$, a chemically ordered structure is obtained such that P is coordinated to Si and vice versa, while the excess of either of the components present in any composition will be coordinated to their own kind. Since P and Si are 3- and 4-connected, a glass with a composition 3 $SiO_{4/2}$/4 $POO_{3/2}$ (=2 P_2O_5) marks the stoichiometric proportions. When $SiO_2/P_2O_5 > 3/2$ in the compositions, there will be additional Si−O−Si bonds, along with Si−O−P bonds. When the ratio is less than 3/2, there will be P−O−P bonds in the structure. An examination of the compositions in Table

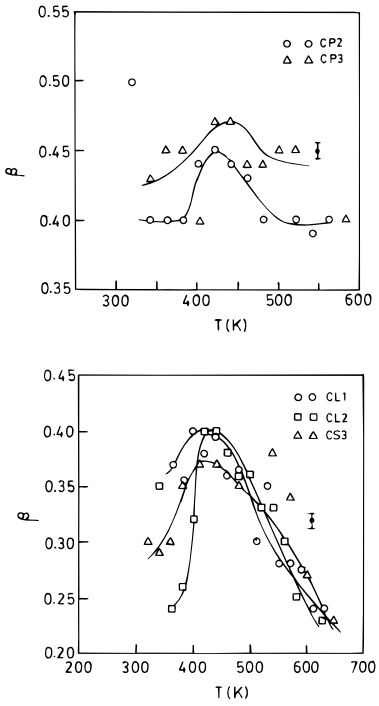

Figure 13. Stretching exponent, β, versus temperature of lithium silicophosphate glasses. The continuous line are guide to the eyes.

1 suggests that the present glasses are all rich in silica and contain Si−O−Si bonds in addition to Si−O−P bonds and that P−O−P bonds are absent. Such is the idealized structure of pure silicophosphate glass.

As $LiNO_3$ decomposes and gives rise to Li_2O in the glasses, the O^{2-} ions cause modification of the ideal silicophosphate structure. The modification occurs on Si−O−P bonds (links) and not on Si−O−Si bonds, as we can infer from a consideration of the partial charges present on the atoms in the two types of links. Partial charges have been calculated using Sanderson's (see the Appendix) procedure,[52] which is based on the principle of electronegativity equalization and are shown below.

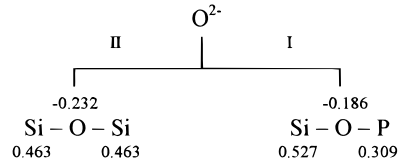

It is evident that the O^{2-} which has to arrive at the site of modification experiences a reduced Coulombic repulsion and increased Coulombic attraction with the Si−O−P bond than with the Si−O−Si bond. Thus the modification occurs on the Si−O−P links and leads to the formation of $(SiO_{3/2}O)^-$ and $(POO_{2/2}O)^-$. Once the chemical reaction is over, the situation is such that an $(SiO_{3/2}O)^-$ (ϕ_3) group and (unmodified) P_3 groups are in intimate contact. But the molecular electronegativities of these two groups are significantly different. Such a difference in electronegativities is indeed equivalent to local free energy differences and leads to a bond-switching reaction, resulting in product species with a mitigated electronegativity difference. As a result, the

(52) Sanderson, R. T. Polar Covalence, Academic Press: New York, 1983.

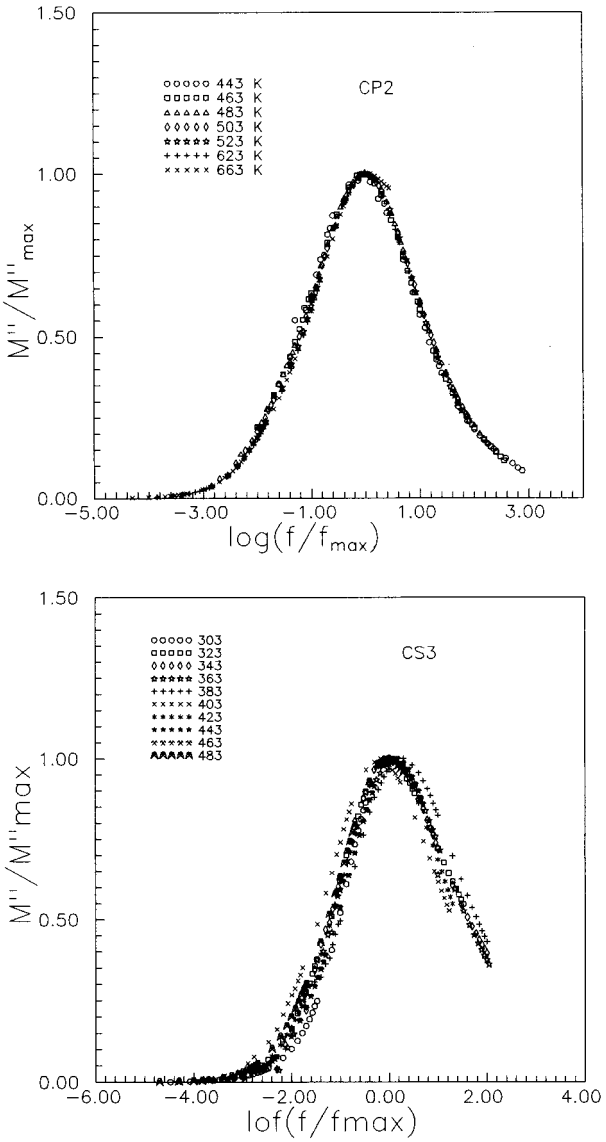

Figure 14. M''/M''_{max} versus $\log(f/f_{max})$ plots for CP2 and CS3 glasses.

following reaction takes place

$$P_3 \;(3.03) + \phi_3 \;(2.11) \rightarrow P_2 \;(2.39) + \phi_4 \;(2.77)$$

The net consequence of this reaction is that the modification results in the restoration of ϕ_4 and formation of another P_2. Silica in the glass is left unmodified. Continued modification will result in complete conversion of P_3 to P_2, as the Li_2O concentration is increased to a level where $R = 1$ or $Li_2O/P_2O_5 = 1/1$ in the glass. The structure now looks like a modified metaphosphate chain in which every alternate P_2 link has been substituted by n ϕ_4 units.

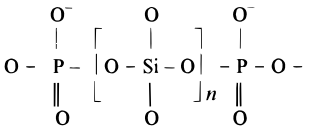

n depends on the ratio of SiO_2 to P_2O_5 in the structure. When R exceeds 1.0, modification is expected to proceed to the next stage with opening up of Si−O−Si in

preference to Si−O−P bonds. This is because of the partial charge distribution shown below for the two situations.

$$\underset{0.463}{\overset{-0.232}{\text{Si}-\text{O}-\text{Si}}}\underset{0.463}{} \quad (\phi_4 - \phi_4)$$

$$\underset{0.363}{\overset{-0.305}{\text{Si}-\text{O}-\text{P}}}\underset{0.160}{} \quad (\phi_4 - \text{P}_2)$$

Surprisingly, we have seen from the NMR spectra presented earlier that Si is present exclusively as ϕ_4. This is possible only if the resultant $(SiO_{3/2}O)^-$ is reconverted to ϕ_4 either by a bond-switching mechanism with an existing P_2 unit or by conversion of $(SiO_{3/2}O)^-$ into $[SiO_{3/2}OH]$. Since the molecular electronegativities of ϕ_3 (2.11) is lower than that of P_2 (2.39), the former process is unlikely. We recall here from IR spectra that the glasses contain uneliminated P−OH groups which give rise to a sharp peak at around 2400 cm^{-1} and whose intensities decrease rapidly as the Li_2O to P_2O_5 ratio increases above 1.0. It is therefore possible that an essentially P_2 unit of the type $POO_{2/2}(OH)$ ($\equiv P_3'$) present in the glass and having a molecular electronegativity of 2.847 reacts with ϕ_3 (2.11), producing ϕ_4' of the type $(SiO_{3/2}OH)^0$ (2.668) and P_2 with a electronegativity of 2.39. [We prefer to designate it as P_3', although the third connection is terminated by addition of proton (−OH in place of −O). This will make the designation of the species more related to the charge it bears than to the extended lattice connections. But such designation has advantages for the present work.] This would be consistent with the fact that only ϕ_4 resonances are seen in the NMR. But this requires a significant proportion of POH groups to be present in equilibrium. We recall here that the sols were acidic and contained HNO_3 and therefore P_3' units are expected to be formed by the reaction of P_2 itself with HNO_3. This can occur at the stage of heating the xerogel when elimination of nitrates occurs,

$$\underset{P_2}{2[POO_{2/2}O^-]} + 2HNO_3 \rightarrow \underset{P_3'}{2[POO_{2/2}OH]} + 2NO_2 + O_2$$

In fact, we suggest that a significant number of phosphorus atoms in the gel are hydroxylated in view of the above reaction. However, the Si−O−P in the newly formed $POO_{1/2}(OH)-SiO_{4/2}$ ($P_3'-\phi_4$) is again subjected to modification [compare partial charges on Si(0.481)−O(−0.219)−P(0.217) with the partial charges on Si(0.463)−O(−0.232)−P(0.463)], resulting in the formation of $POO_{1/2}(OH)O^-$ ($\equiv P_2'$). This species may be transient, because it can disproportionate to P_3'' [$\equiv POO_{1/2}(OH)_2$] and P_1 by bond switching,

$$2[POO_{1/2}(OH)O]^- \leftrightarrow [POO_{1/2}(OH)_2] + [POO_{1/2}O_2]^{2-}$$

$$2P_2' \leftrightarrow P_3'' + P_1$$

But P_3'' is likely to be consumed by ϕ_3 to produce ϕ_4' and P_2',

$$[SiO_{3/2}O]^- + [POO_{1/2}(OH)_2] \rightarrow [SiO_{3/2}OH] + [POO_{1/2}(OH)O]^-$$

$$\phi_3 + P_3'' \rightarrow \phi_4' + P_2'$$

The disproportionation reaction alone can provide P_1, which is observed experimentally in some of the glasses only. The disproportionation may be driven by the prospect of generating higher entropy with a singly connected P unit in the structure. The newly created P_3'' may lead to a second stage condensation with ϕ_4', producing normal P_3' and ϕ_4. We feel that this is perhaps the only facile way in which pyrophosphate species, P_1, could be produced in the glasses. It is also obvious that when the *R* values exceed 1.5, fairly complex equilibrium of species occur. However, finally the modification process results in the formation of only P_2 and P_1 species. If the modifier concentration is low, unmodified P_3 species will remain as in CP and CL series of glasses. Hence the entire process of modification occurs with only the P units and not with ϕ_4 units. Given in Table 6 are the expected structural species from purely stoichiometric considerations. However, in CL1 and CL2, where only P_1 species are expected to be produced, the equilibration reactions discussed above dominate and lead to the formation of P_2 species also. P_3 in these glasses may only be P_3'. However, further direct confirmatory evidence is needed to support the mechanisms suggested above, and therefore, exact proportions of P_1, P_2, and P_3 have not been determined in this work.

Structural Model and the Observed Properties. The presence of Si−OH groups and P−OH groups has the effect of expanding the amorphous lattice, because of reduced cross-linking and an effective addition of water molecules. This manifests in a significant positive difference between the observed molar volumes and weighted linear sums of the molar volumes of glassy SiO_2, P_2O_5, and crystalline Li_2O. The OH groups attached to Si and P produce the infrared features referred to earlier at 3400 and 1650 cm^{-1} for SiOH and 2400 cm^{-1} for POH. As expected from the reactions discussed earlier, POH groups are continuously eliminated as the Li_2O/P_2O_5 ratio increases significantly above unity. This is the reason for the reduced intensities of 2400 cm^{-1} in the infrared spectra. It is well-known that IR extinction coefficients of the hydroxyl groups are very high, and therefore, corresponding peaks in the IR spectra produce pronounced absorption features. Several of the glasses examined through differential scanning calorimetry (DSC) (Figure 2) revealed the presence of small endothermic features at ~400 and 523 K, and the energies associated with them are typically on the order of 120 cal/mol or less, which can only be associated with the evaporation of less than 1.5 mol % of adsorbed water. It is, therefore, evident that the infrared features are not attributable to any uneliminated water present as bonded molecular water.

The single NMR resonance of Si is attributed to ϕ_4 and ϕ_4' ($\equiv SiO_{3/2}OH$) present in the glass, and the P resonances arise from various P_3, P_2, and P_1 species grouped according to their chemical shifts in Table 4. All NMR features are in complete accordance with the model.

Table 6. Ratio Nonbridging to Bridging Oxygen (NBO/BO) for Various Compositions of Silicophosphate Glasses

glass code	structural species			NBO/BO	(NBO/BO) × (P/2P + S)
	P3	P2	P1		
CP1[a]	20	20			
CP2	10	30		0.33	0.126
CP3	0	40		0.50	0.200
CL1	0	0	20	2.00	0.444
CL2	0	20	10	0.80	0.253
CL4[a]	10	40			
CS3	0	30		0.50	0.150

[a] Protonic conduction.

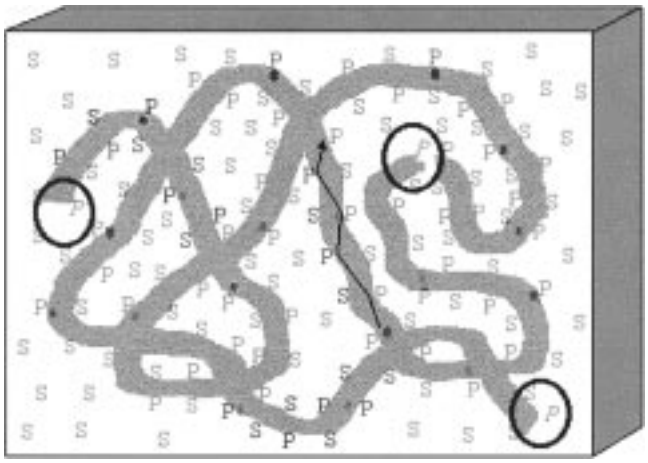

Figure 15. One-dimensional tubular conducting pathways for Li^+ ion motion in silicophosphate glass matrix. S denotes a silica unit, P denotes a P_2 unit, and *P* denotes a P_1 unit. The small circles indicate Li^+ ions. Hopping of Li^+ ions from one P site to another is shown.

The conductivities of the glasses arise from the motion of Li^+ ions which are located in the vicinity of the charged phosphatic species present in the glass. From the model, we expect that this occurs along the S−P−S chains (here we designate the silicate and phosphate units as S and P, respectively). These chains, however, consists of two or three S groups bunched together at some points which increases inter-Li^+ ion distances. Also the chain can be interrupted by the presence of a pyrophosphate moiety (P_1 units). The conductivity itself is most likely a one-dimensional transport phenomenon where the Li^+ ions hop distances corresponding to no more than 3−4 Å on the P−S−P−S chains. Two or more strands (of ...P−S−P−S...) line up along connected paths with staggered P−S−P−S positioning along the walls of a "noodle pipe" inside which Li^+ ions are located. Li^+ ions hop from P to P centers, which are now much closer than on a single chain. This structure of the conduction channel is almost reminiscent of Greaves'[53] description of a modified random network, except that the model here provides naturally for the closeness of the charged centers on P−S−P−S chains. This has the effect of reducing the actual volume of the glass effectively used by Li ions for transport, as argued earlier. Such a one-dimensional charge transport in silicophosphate glass is visualized as shown in Figure 15. Two features of Li^+ ion transport are therefore self-consistent: (a) the virtual increase in Li^+ ion concentration leads to low values of β typical of fast ion conductors[48] and (b) the potentials along the one-dimensional silicophosphate tubes do not vary very much and hence the almost similar activation barriers (0.64−0.71 eV) as seen in Table 2. Although the presence of P_1 species interrupts the covalent chains, the average barrier may not be affected because the two O^- centers on phosphorus may lock up a Li^+ ion, thereby restoring the uniformity of the potentials along the tubes. For the same reason, the variation in the observed dc conductivities is within an order of magnitude, despite the wide range of glass compositions. In fact, both the activation barrier and conductivities are therefore a function of only the ratio of nonbridging oxygen to bridging oxygen and somewhat modified by the dilution effect of the silica matrix. The latter is accounted for by a ratio of P_2O_5 to SiO_2. The expected variations of both σ_{dc} and E_a are represented in Figure 7b. The implications of the model are well-supported by the observed linear variations.

The ac conductivity and the relaxational behavior represent the local jumps of the ions between equivalent positions, which give rise to polarization currents. The tubular structure of the conducting portion of the glass in the model locates the positions of the Li ions into two distinct classes, one associated with P_2 type of defects and the other with P_1 type of defects (P_3, being a neutral species, is not of relevance in defining the ion conduction pathways). The available equivalent positions around the NBO's in the two situations are likely to be affected by the distances between the potential wells, by the occasional OH groups, and by the chain interruption due to the presence of ϕ_4 groups. OH and ϕ_4 groups occur randomly in the structure. It is therefore expected that the relaxation times characterizing the two types of sites can be different. Therefore, even if the diffusion coefficients and jump distances are similar, one would expect different *s* values. Correspondingly, in the ac conductivity behavior, the net influence of the two *s* values will manifest. The effect of distinct local relaxation times associated with P_1 and P_2 type sites is more clearly manifested in β values. We notice two distinct groups of β values, bunched around 0.24 and 0.45. However, we did not observe any distinct relaxation peaks, which again suggests that there exists a single peak relaxation time whose width is modified by virtue of the spread in the local potential well structure.

It is seen from a simple consideration of the partial charge of hydrogen in $(SiO_{3/2}(OH))^0$ and $(PO_{1/2}(OH)O)^-$ that the OH group attached to Si is more acidic than that in POH. But both of them are significantly less acidic because they carry partial charges of 0.251 and 0.196, respectively. Therefore, we do not expect much protonic conductivity, although it appears to be dominant in CP1 and CL4 at low temperatures, even though the glasses were dried up to 673 K before the conductivity measurements. We do not clearly understand this feature at present.

It is therefore evident that silicophosphate glasses possess a fascinating structure. The observed properties of silicophosphate glasses are all a consequence of exclusive association of nonbridging oxygens with P and formation of one-dimensional tubular conducting pathways spanning the entire structure.

(53) Greaves, G. N.; Fontaine, A.; Lagarde, P.; Raoux, D.; Gurman, S. J. *Nature* **1981**, *293*, 611.

Appendix

Sanderson's Procedure To Calculate the Average Electronegativity of Anions Present in the Glasses. The effective electronegativity (χ_{eff}) of an anion of the type $[M_mO_n]^{x-}$ is determined as given below.

(a) The partial charge on the constituent atoms M (Δ_M) and O (Δ_O) are evaluated as

$$\Delta_M = (\chi_{eff} - \chi_M)/(\Delta\chi_M) \qquad \Delta_M\Delta\chi_M = \chi_{eff} - \chi_M \quad \text{(A.1)}$$

$$\Delta_O = (\chi_{eff} - \chi_O)/(\Delta\chi_O) \qquad \Delta_O\Delta\chi_O = \chi_{eff} - \chi_O \quad \text{(A.2)}$$

where $\chi_A = 1.56\sqrt{\chi_A}$ (A = M or O) and χ_M and χ_O are the electronegativitites of M and O atoms, respectively.

(b) The net charge on the anion is equated to the sum of the partial charges on each atom present in the anionic groups as

$$m\Delta_M + n\Delta_O = -x \quad \text{(A.3)}$$

By solving eqs A.1−A.3, χ_{eff}, Δ_M, and Δ_O are evaluated.

Example. The effective electronegativity (χ_{eff}) of $[POO_{2/2}O]^-$ is determined as follows: the electronegativity values used are 2.19 and 3.44 for phosphorus and oxygen, respectively. The partial charges on the phosphorus atom is given by

$$\Delta_P = (\chi_{eff} - \chi_P)/(\Delta\chi_P) = (\chi_{eff} - 2.19)/(2.308)$$

$$\chi_{eff} - 2.308\Delta_P = 2.19 \quad \text{(A.4)}$$

Partial charges on oxygen are given by

$$\Delta_P = (\chi_{eff} - \chi_O)/(\Delta\chi_O) = (\chi_{eff} - 3.44)/(2.893)$$

$$\chi_{eff} - 2.893\Delta_O = 3.44 \quad \text{(A.5)}$$

Also from the charge neutrality principle,

$$\Delta_P + 3\Delta_O = -1 \quad \text{(A.6)}$$

Solving eqs A.4−A.6 yields

$$-6.924\Delta_O - 0.118 = \chi_{eff} \quad \text{(A.7)}$$

$$2.893\Delta_O + 3.44 = \chi_{eff} \quad \text{(A.8)}$$

Solving eqs A.7 and A.8 provides

$$\chi_{eff} = 2.39$$

$$\Delta_P = 0.087$$

$$\Delta_O = -0.362$$

Acknowledgment. We thank the Commission of the European Communities for the financial support.

CM980216O